Homework 3

Joseph Le

AAE 575

31 October 2021

Problem 1:

Part 1:

The pseudorange can be calculated with the data given in two different ways. One way is to use the pseudoranges on L1 and L2 which combine to create an ionosphere free pseudorange, and the other way to compute the pseudorange is to use the carrier phase. To calculate the ionosphere free pseudorange using the L1 and L2 pseudoranges the equation on page 292 of the notes will be used with the L1 and L2 pseudoranges plugged into their respective parts. The carrier phase ionosphere free pseudorange can be calculated using the definition of the carrier phase equation which is given in equation 5.32 in combination of equation 5.33 of the textbook. The geometric ranges were also calculated using the Pythagorean theorem along with the given values for range and position. The discrepancies between the pseudoranges stem from the fact that the ionosphere free pseudorange does not consider the ionospheric delays as is suggested in the name, thus there is a discrepancy between the pseudorange calculated by the L1 and L2 pseudoranges. The large difference that is seen in the carrier phase pseudoranges come from the integer ambiguity in the carrier phase where it is unknown which cycle/phase in the carrier phase we are in. The relationships between the three ranges can be seen in figure 1.

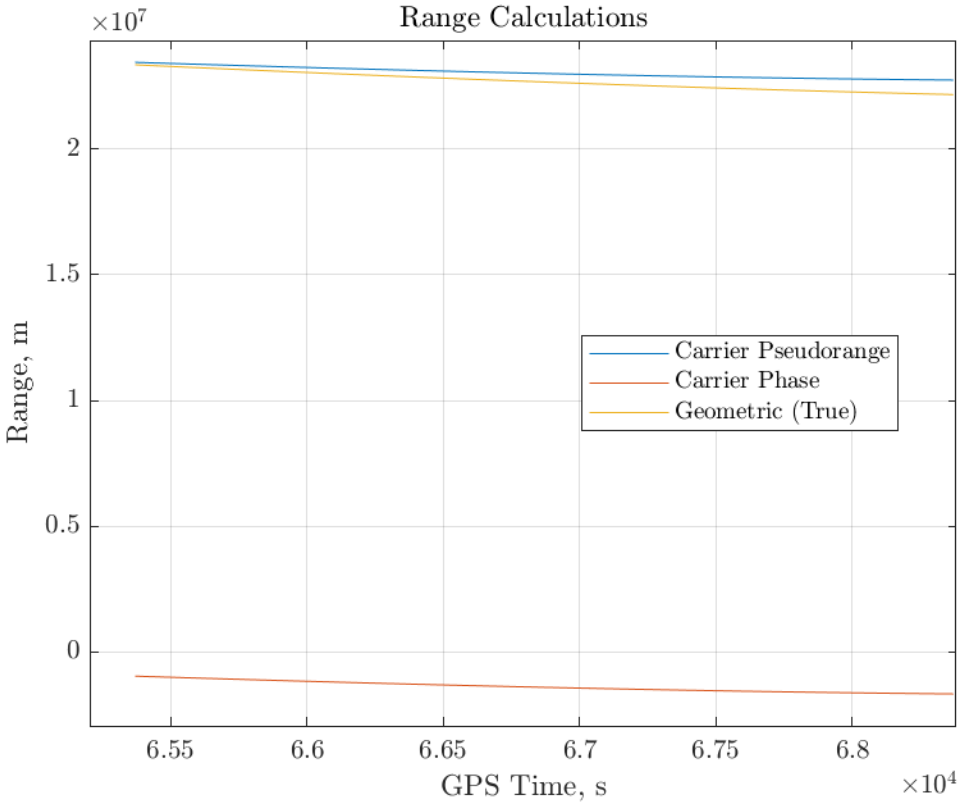

Figure 1 – Range Calculations

The range rates were also calculated for the carrier phase and carrier pseudorange by using the difference function in MATLAB then interpolating the output to fit it to the GPS time in order to plot. An additional parameter, doppler, can be used to calculate the range rate as well. This is done by taking the time derivative of the pseudorange equation to give the doppler equation and modifying the previous equations include doppler. The four plots can be seen in figure 2 below. Similar to the ranges, the discrepancies between the measurement calculations and the geometric range rates originate from the "ionosphere free" part of the equations.

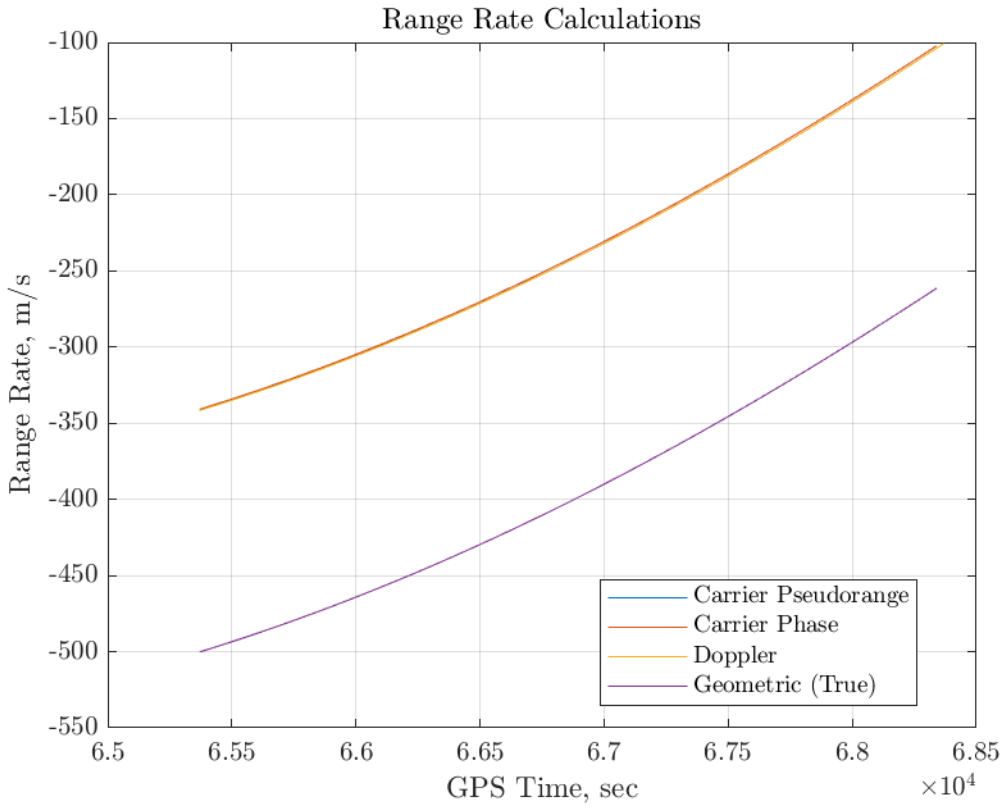

Figure 2 – Range Rate Calculations

Part 2:

Using the doppler measurements for L1 and L2, the oscillator frequency bias can be calculated. This is derived from the doppler frequency equation on page 242 of the notes as the oscillator frequency bias is solved for. To get the equivalent line-of-sight velocity bias, the oscillator frequency bias is multiplied by the wavelength of each carrier frequency. Doing these calculations and plotting them the values for L1 and L2 against each other, it can be seen in the plots below that the L1 bias is compatible with the L2 bias since they are extremely close to each other as seen in both figures 4 below which shows the that the rates that the clock drifts is nearly the same for L1 and L2. The two figures below include the plots for the oscillator frequency bias over time and the line-of-sight velocity bias over time.

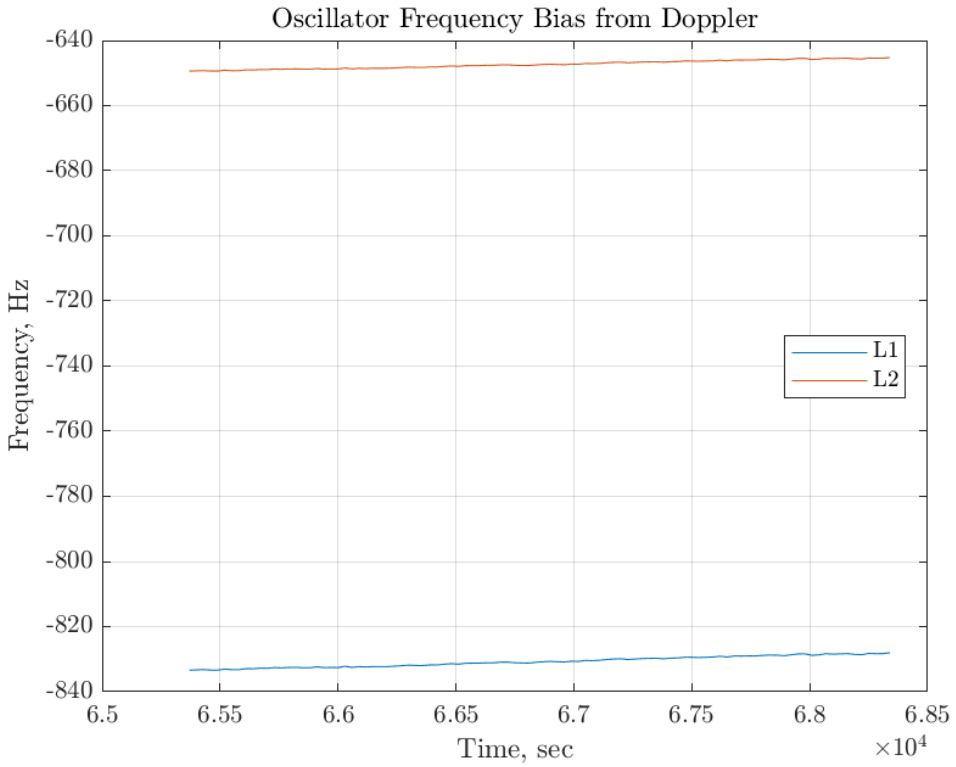

Figure 3 – Oscillator Frequency Bias from Doppler

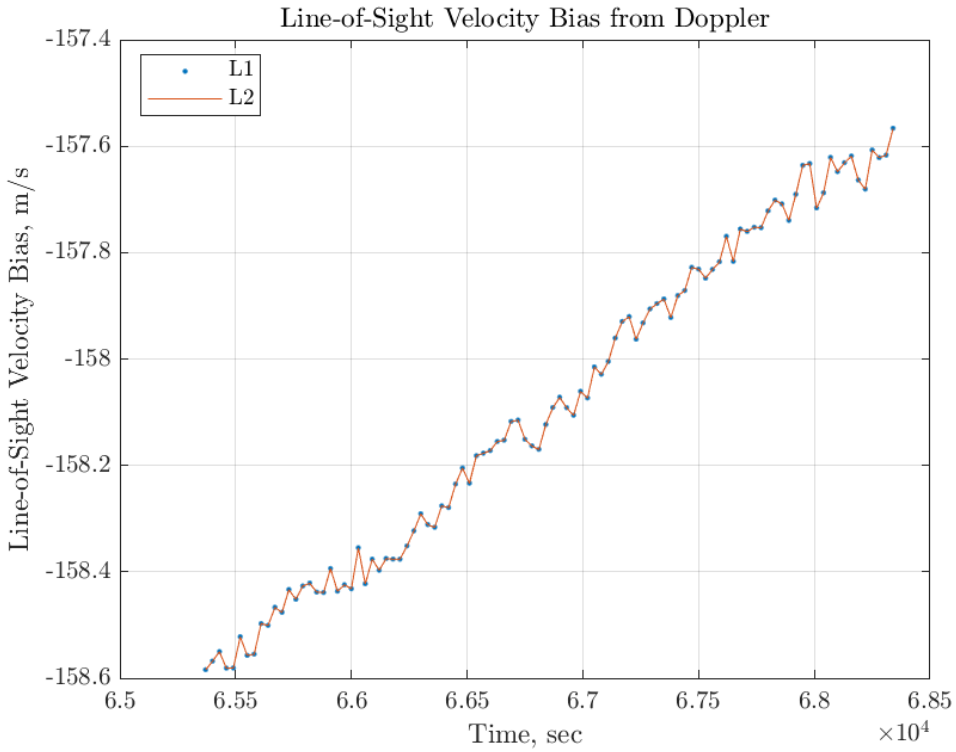

Figure 4 – Line-of-Site Velocity Bias from Doppler

Part 3 & 4:

In the same vein, the receiver clock biases and its rates can also be calculated using the ionosphere-free pseudorange and the ionosphere-free carrier phase measurements. As for the pseudorange measurements, the clock bias is just the difference between the measurement and the true geometric range that was calculated, this gives the clock bias in terms of meters. Similarly, the clock bias for the carrier phase measurements can be calculated in the same way using the respective carrier phase ionosphere free pseudorange. Similar to part 1, the rates for these measurements are done by using a difference equation on the input vector and interpolating it to fit into the GPS time for plotting. The plots for the clock biases and the clock bias rates can be seen below in figure 5 and 6. In figure 5, there is a large difference between the carrier phase and pseudorange measurement calculations, this comes back to the fact that there is an integer ambiguity that was not taken into account for which results in the large discrepancy. However, this is okay since the clock bias rates are within the same order of magnitude and seem to line up fairly well as seen in figure 6.

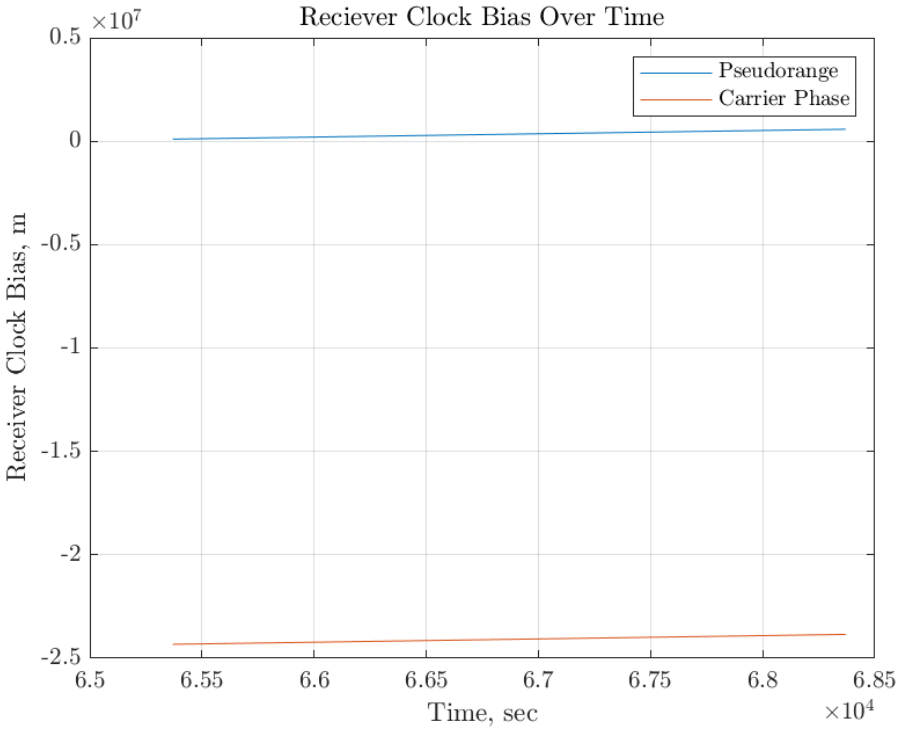

Figure 5 – Receiver Clock Bias

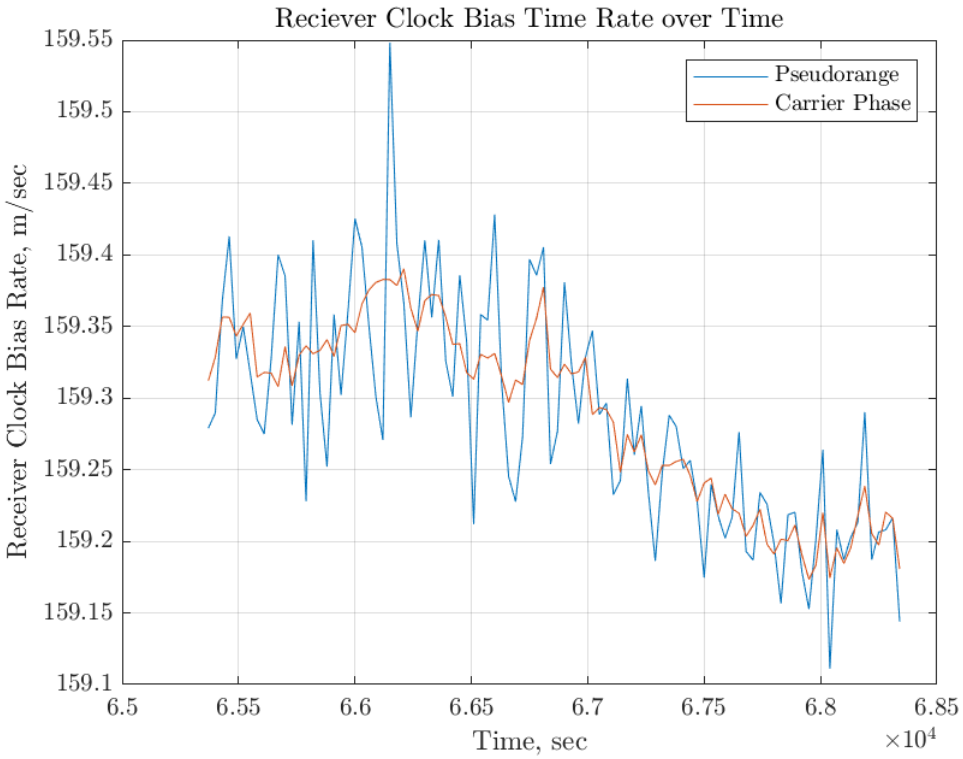

Figure 6 – Receiver Clock Bias Rate

Part 5:

Using the range rates that were calculated in part 1, the frequency error can be computed at each step for the three measurements. This is done by taking the difference between the negative of the pseudoranges (calculated from the measurements), divided by the wavelength of the two carrier frequencies, and the respective carrier doppler frequency. Plotting both the L1 and the L2 responses on separate plots (figures 7 and 8), it can be seen that the L1 and L2 plots are nearly identical so discussion on the stability will be made using the L1 plot.

It can be seen in figure 7 that not all of the measurements give the same results. The doppler has a slight increase (positive slope) while the carrier phase and pseudorange calculations both demonstrate a slight decrease (negative slope) and both of them are fairly close to each other. This means that the oscillator behavior isn't completely constant and may be a problem. Since the pseudorange and carrier phase frequencies drift in the negative direction over time while the doppler frequencies drift positive over time, it the differences in the frequencies continue to grow. Since stability is a measurement of how well the oscillator can maintain a set constant frequency, the drift that is present in the frequencies may mean that the oscillator may be slightly unstable.

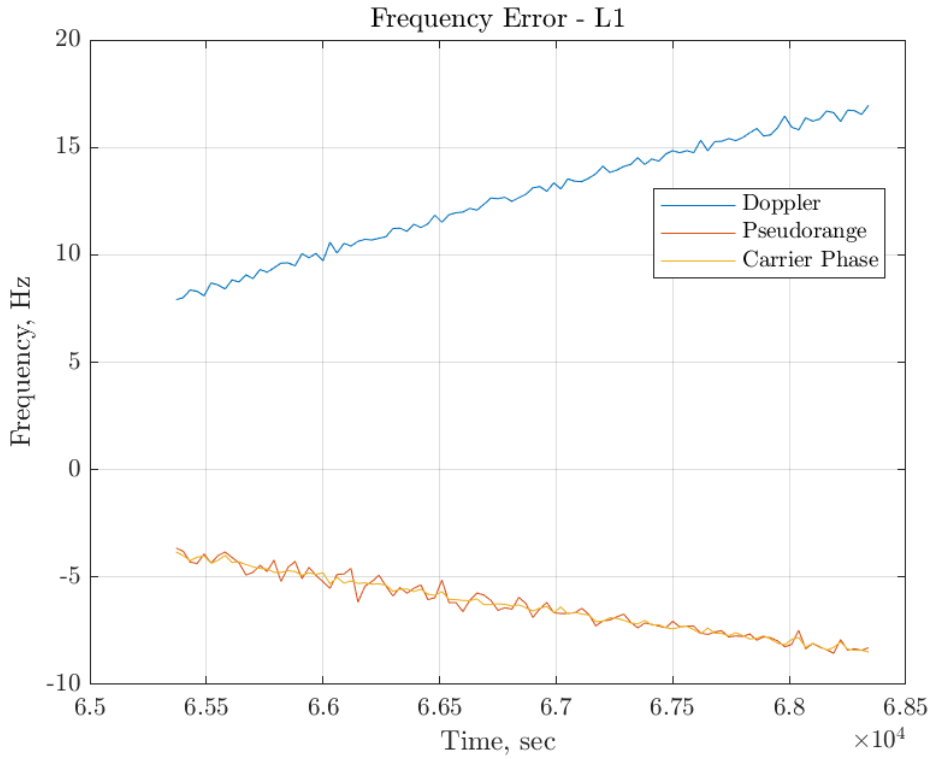

Figure 7 – Frequency Error on L1

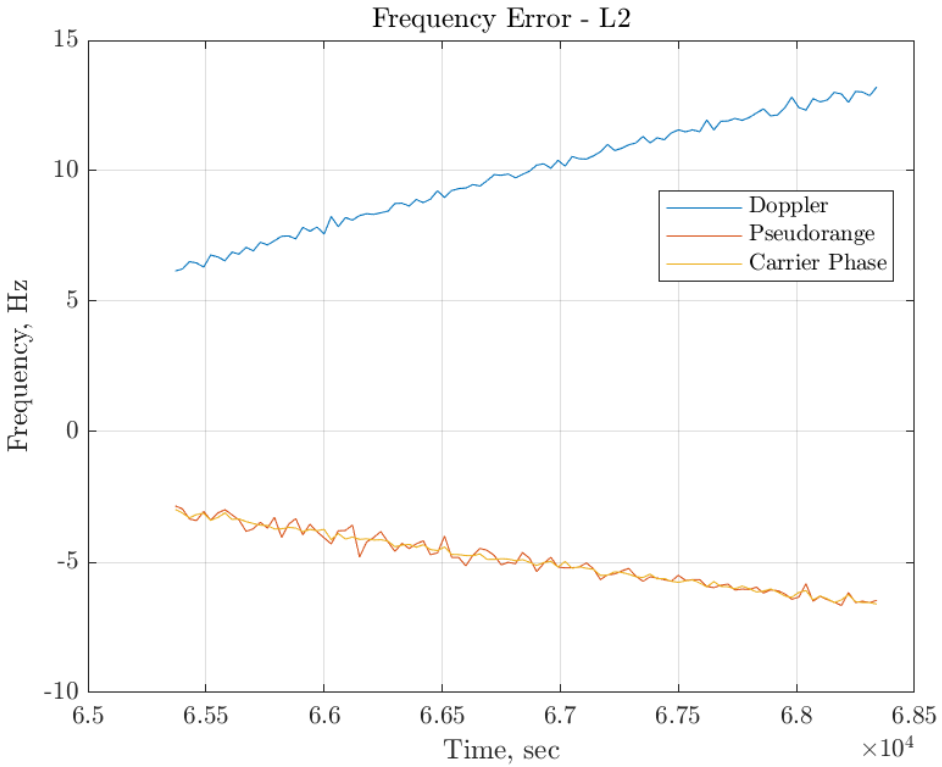

Figure 8 – Frequency Error on L2

Problem 2:

Using the dual frequency data and the alpha and beta values given in the table, the Klobuchar model could be used to estimate the ionospheric delay that is perceived in the data. To do this, an angle, psi, which is between the vector from the center of the Earth to the receiver and the center of the Earth to the Ionosphere pierce point. This angle is then used to calculate the IPP's (ionosphere pierce point) location in latitude and longitude using an approximation given in page 304 of the class notes. These coordinates are then used to calculate the geomagnetic latitude of the IPP which also used an approximation. The geomagnetic latitude is then used to calculate the A2 and A4 coefficients for each time step using the alpha and beta value as well in a 3^{rd} order series found on page 306 of the notes. Once the coefficients are found, the Klobuchar model can then be implemented, and the local time can be calculated. This gives the delay at the zenith (vertical delay), which will be multiplied by an obliquity factor that is calculated using the elevation, this gives the final ionospheric delay using the Klobuchar model which is seen below plotted against the local time. The model plotted below using the data that was given with the L1 carrier.

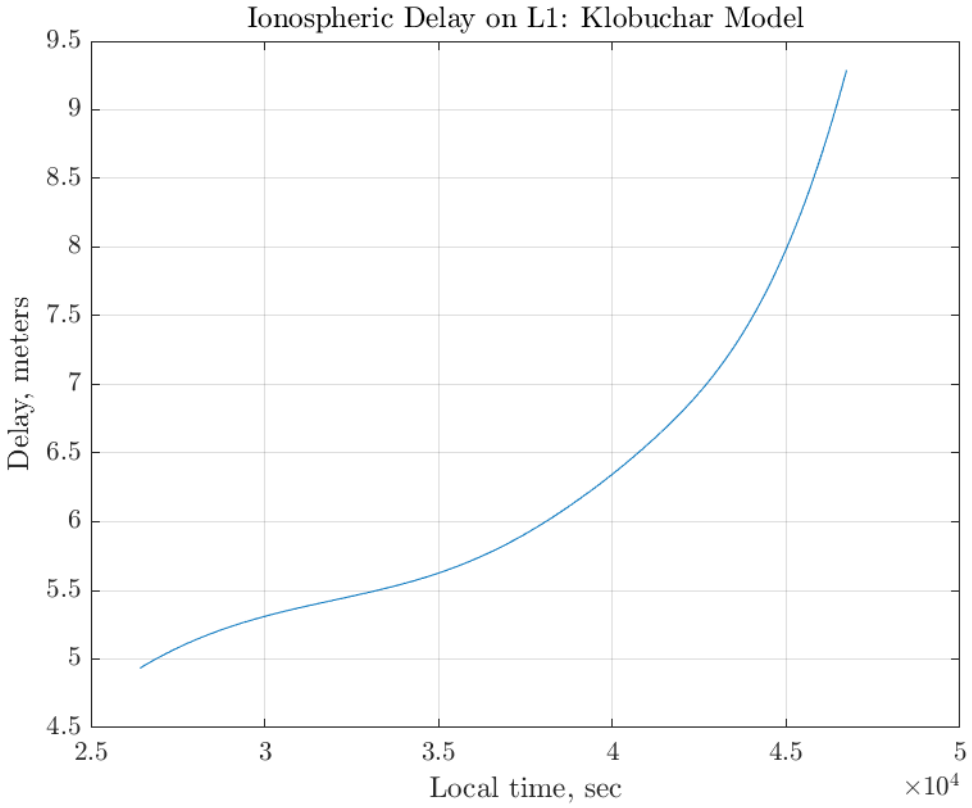

Figure 1 – Klobuchar Model Delay on L1

Problem 3:

Using the same data set of problem 2, the ionospheric delay at the L1 frequency could also be calculated using the pseudorange measurements for L1 and L2. To do so, the dual frequency method can be used. This makes use of the values for the frequencies of L1 and L2 to get A which is the squared value of the frequency of L1 divided by the difference between the squared values of L1 and L2 frequencies. Then, using equation 5.30 from the book, the ionospheric delay on L1 can be calculated directly (there is also other equation in 5.30 that can be used in this case). The ionospheric delay on L1 is plotted below against the Klobuchar model. As seen in the plot, the dual frequency/pseudorange method is much more erratic, which makes sense because it is said to be much more accurate and gives a truer delay since it is using fundamental plasma physics to calculate the delays which takes into account fluctuations and irregularities in the ionosphere. On the other hand, the Klobuchar model gives a much smoother estimation because it is a lower order model used for older receivers and is less taxing on hardware.

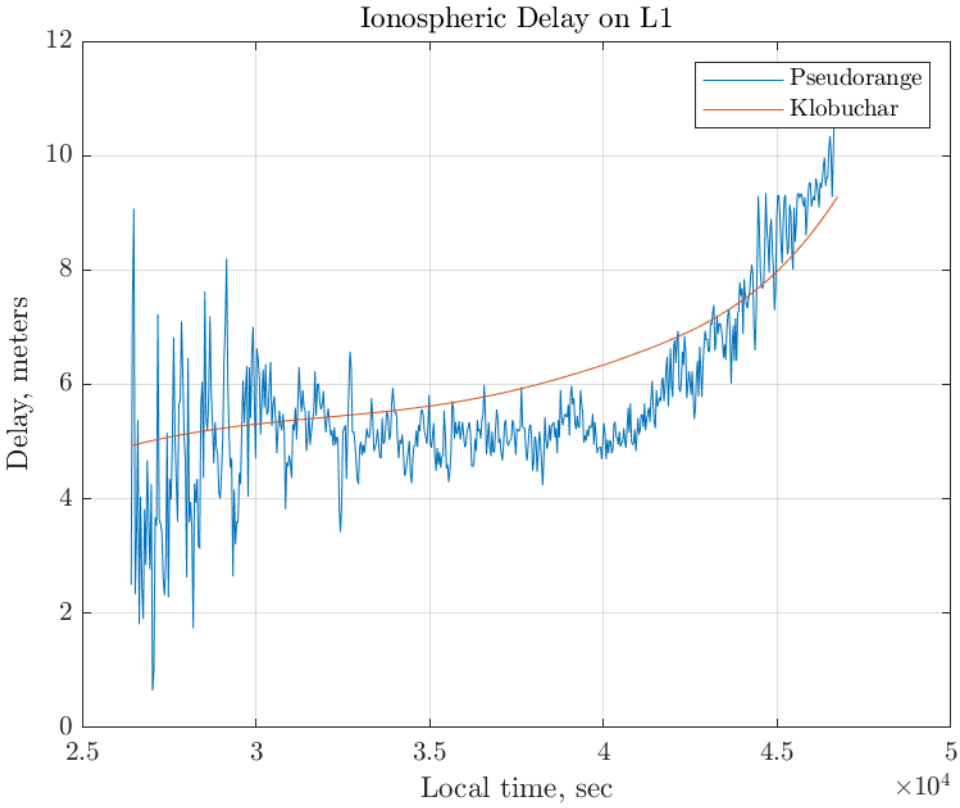

Figure 2 – Ionospheric Delay at L1 (Klobuchar vs Pseudorange)

Problem 4:

Both the Saastamoinen and Hopefield models separate the delays for the model between the "wet" and "dry" parts of the troposphere.

For the Saastamoinen model, which was derived from ideal gas laws, the zenith delay for the dry troposphere uses the latitude on the Earth of the test station, the orthometric height of the station, and the total pressure at the test station, these values are then plugged into equation 5.39a in the textbook. Similarly, equation 5.39b gives the zenith delay for the wet section of the troposphere using the surface temperature at the station and the partial pressure due to water at the station.

The Hopfield model is another model for the troposphere which uses the same parameters and introduces two new parameters which are the respective heights of the dry and wet layers of the troposphere. The dry layer height is calculated using the equation at the bottom of page 317 of the course notes which uses the surface temperature, and the wet layer height is assumed to be

a constant 11000m. These values are then plugged into equations 5.41a and 5.41b in the textbook to get the zenith delays for both the dry and wet sections of the troposphere respectively. Below are plots of all the tropospheric delays on one plot, and two separate plots of the dry and wet delays comparing the two models to get more detail.

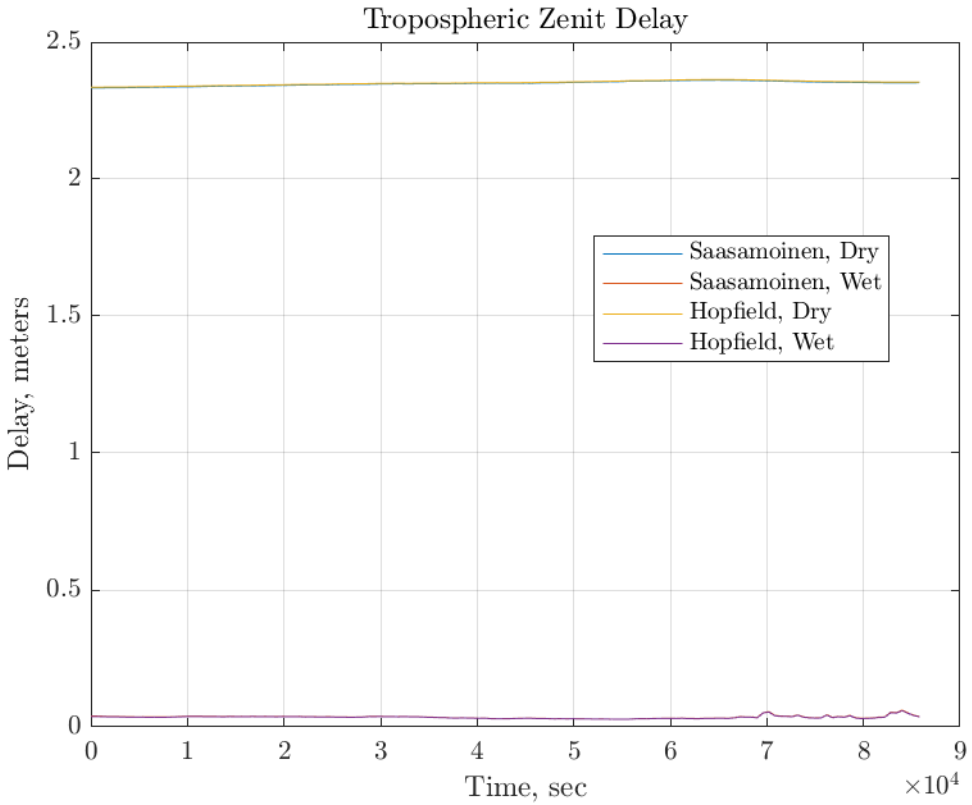

Figure 3 – Zenith Tropospheric Delay (wet & dry) – Saastamoinen and Hopfield

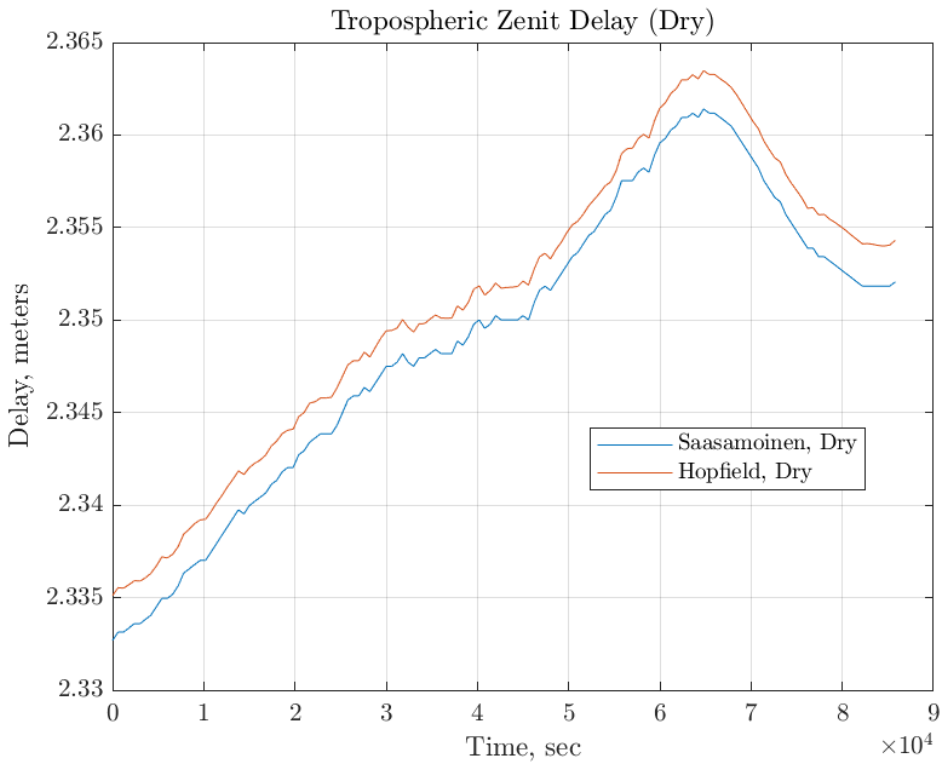

Figure 4 – Dry Zenith Tropospheric Delay – Saastamoinen and Hopfield

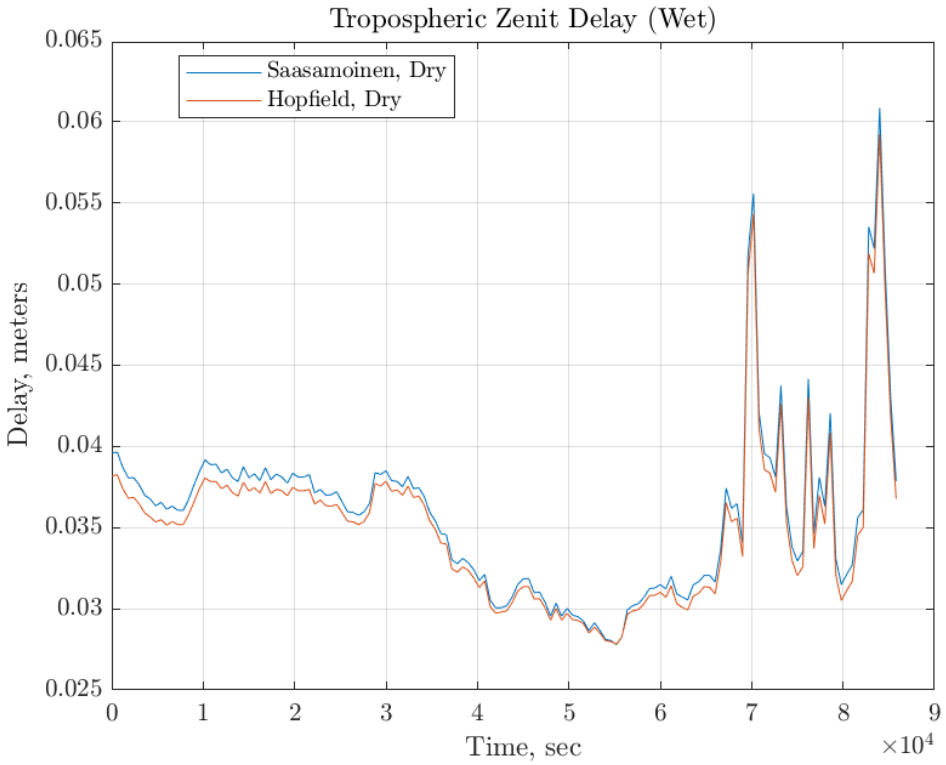

Figure 5 – Wet Zenith Tropospheric Delay – Saastamoinen and Hopfield

Problem 5:

In problems 3 and 4, the zenith delays were found for the troposphere, meaning it is only the delay due to the troposphere going in a radial direction from the center of the Earth. Since GPS satellites can be at angles compared to a receiver on the surface of the Earth, mapping functions (similar to the obliquity function for the ionosphere) must be used. These mapping functions all take the satellite elevation as an input and return the mapping function. The first mapping function is the flat-Earth mapping function which is given on the homework sheet. The flat-Earth mapping function is bad as the elevation decreases and is very inaccurate at elevations below 15 degrees, this mapping function is applied to both the wet and try delays. The second mapping function is slightly more complicated and can be found in equation 5.42 in the textbook. Similarly, this mapping function will be applied to both the dry and wet delays. Finally, the Chao mapping functions can be found in page 324 of the course notes. Unlike the two previous mapping functions, the Chao mapping functions have separate equations for the wet and dry parts of the delay. The plots for the total tropospheric delays can be seen in figures 6 through 9 where the dry and wet zenith delays are combined using the mapping functions.

As seen in the plots below, the flat-Earth mapping function does not do well when the satellite is at a low elevation as it is very separated from the other two models. The fact that the flat-Earth model slowly converges with the other two models as the elevation increases while the other two models stay relatively close to each other suggests that the flat-Earth model is inaccurate and is only accurate at much higher elevations while, on the other hand, other two models are much more accurate in a larger range of elevations, with the Chao mapping model being more accurate than the Misra/Enge mapping model.

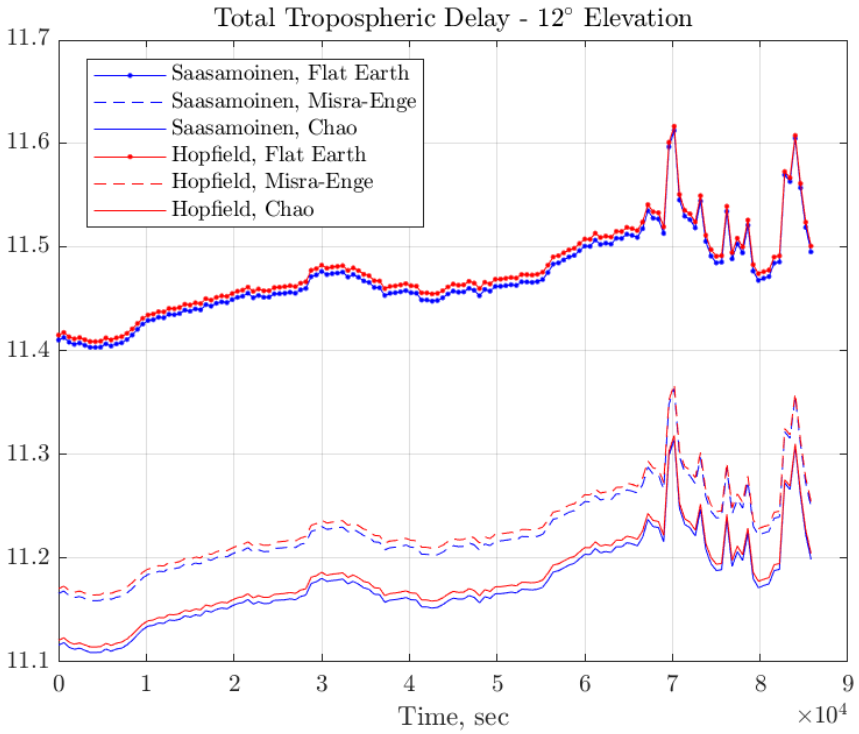

Figure 6 – Total Tropospheric Delay – 12 Degrees

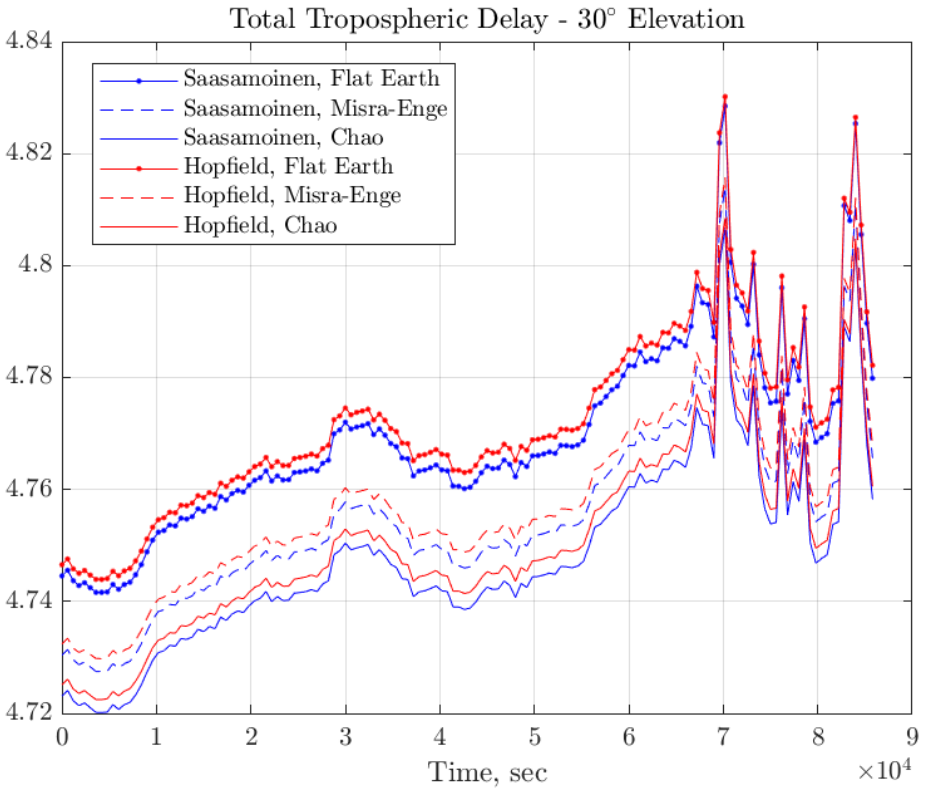

Figure 7 – Total Tropospheric Delay – 30 Degrees

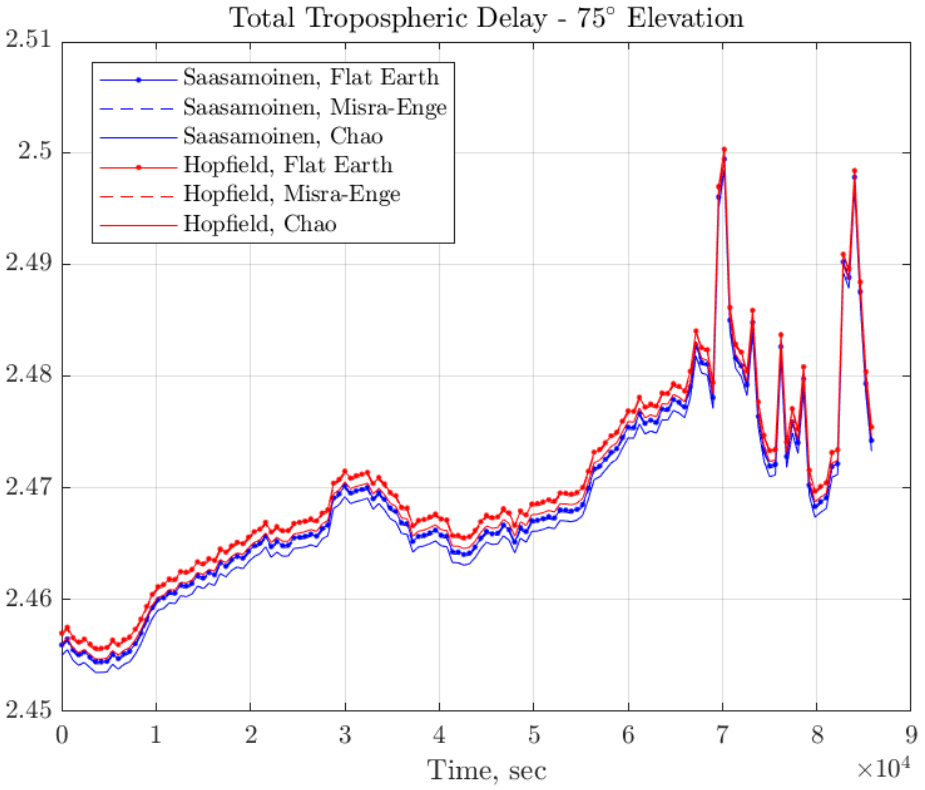

Figure 8 – Total Tropospheric Delay – 75 Degrees